Available online at www.sciencedirect.com
SCIENCE DIRECT®
Journal of Solid State Chemistry 174 (2003) 141–151
JOURNAL OF SOLID STATE CHEMISTRY
http://elsevier.com/locate/jssc

# Atomistic modelling of the hydration of $CaSO_4$

Craig D. Adam*

*School of Chemistry and Physics, Keele University, Keele, Staffordshire ST5 5BG, UK*

Received 19 December 2002; accepted 30 March 2003

**Abstract**

Atomistic modelling techniques, using empirical potentials, have been used to simulate a range of structures formed by the hydration of $\gamma$-$CaSO_4$ and described as $CaSO_4 \cdot nH_2O$ ($0 < n < 1$). The hemihydrate phase ($n = 0.5$) is of commercial importance and has been subjected to much experimental study. These simulation studies demonstrate significant water–matrix interactions that influence the crystallography of the hydrated phase. The existence of two types of hydration site has been predicted, including one within the $Ca^{2+}$ coordination sphere. Close correlation between water molecule bonding energy, $Ca^{2+}$–$O_w$ bond length and unit-cell volume have been established. This shows that as the number of water molecules within the unit cell increases, the bonding energy increases and the unit cell contracts. However around $n = 0.5$, this process reaches a turning point with the incorporation of further waters resulting in reduced binding energy and an expanding unit cell.


*Keywords:* $CaSO_4$; Modelling; Simulation; Hemihydrate; Gypsum; Hydration; Cement

## 1. Introduction

Gypsum plasters ($CaSO_4 \cdot 2H_2O$) which are used extensively for building, ceramics, and medical applications, are formed through the hydration of $CaSO_4$ hemihydrate [1]. This material is formed commercially through the partial dehydration of gypsum itself, with complete removal of water resulting in the anhydrous compound, $\gamma$-$CaSO_4$. There is widespread interest in the crystallography, structure, and bonding within these materials, both from the commercial point of view and to understand better the interactions between water molecules and inorganic sulfates which are crucial to the phase behavior in these compounds. Among the key issues are determining how many distinct hydrated phases exist [2,3], their behavior under a variety of thermodynamic conditions [3] and control of the hydration and crystallization process through the use of additives [4,5] and impurity ions [6].

A wide range of experimental techniques, including the X-ray powder diffraction, infrared (IR) spectroscopy, thermogravimetric methods, and microscopy, have been utilized for time-resolved studies or work under conditions of controlled temperature, pressure, or humidity on gypsum materials. However, until now, atomistic modelling approaches have not been applied to these systems. The use of transferable, empirical potentials coupled to lattice energy minimization and related computational techniques, is an established approach to the simulation of the structures and properties of inorganic materials. Anhydrous systems, e.g., Ref. [7] have been the object of much research and the interaction of water with inorganic surfaces such as carbonates [8] or porous systems such as zeolites [9] has been a source of fruitful study.

Modelling of bulk, hydrated solids where the crystallography and properties of the material are closely dependent on water–matrix interactions, have not received much attention, however. Sulfates, in particular calcium sulfates, are excellent systems in which to develop and apply the atomistic modelling approach, as such materials are the basis of a range of modern cementitious materials where bulk hydration reactions and interactions play a leading role in engineering the properties of the final product.

This work is concerned with the application of atomistic modelling techniques, using empirical potentials, to explore the water–matrix interactions in hydrated $CaSO_4$ materials. An appropriate set of

*Fax: +1-782-712378.
*E-mail address:* c.d.adam@keele.ac.uk.

0022-4596/03/$ - see front matter © 2003 Elsevier Science (USA). All rights reserved.
doi:10.1016/S0022-4596(03)00190-7

potentials are derived and validated on known structures. These are then used to simulate various subhydrate configurations and the results compared with experimental data available.

## 2. Crystallography of $CaSO_4$ and its hydrates

The structures of insoluble anhydrite [10] ($\beta$-$CaSO_4$) and gypsum ($CaSO_4 \cdot 2H_2O$) are well understood, the latter having been studied in detail by neutron diffraction [11]. The crystal structure of gypsum is based on a layer structure where two sheets of $SO_4^{2-}$ tetrahedra are intimately bound together by $Ca^{2+}$ ions to form a strong double sheet. These layers are separated and bound by the water molecules, each of which links a $Ca^{2+}$ ion to sulfate oxygens in each layer. Each $Ca^{2+}$ coordination shell contains six sulfate oxygens and two water molecules. The sheets lie perpendicular to the [010] direction.

On the other hand, the phases formed through the dehydration of gypsum—*subhydrate* materials of composition $CaSO_4 \cdot nH_2O$ ($0 < n < 2$) and, ultimately, soluable anhydrite ($\gamma$-$CaSO_4$)—have been the subject of much attention since the pioneering work of Gallitelli [12]. These studies have revealed many discrepancies with respect to both the space group and to the distinct hydration states which exist. Matters have been complicated by the lack of close control of vapor pressure during most experimental work and of course the need, in general, to use powder diffraction methods, preferably with both X-rays and neutrons. There are examples of structures hydrated up to $n = 0.8$ and space groups ranging from monoclinic $I2$ [13] to trigonal $P3_121$ [14].

Notable contributions over recent years include a study on the dehydration of deuterated gypsum, using time-of-flight neutron powder diffraction [15]. Due to sample-dependent peak broadening, this provided only a qualitative structure for the water molecule locations in the hemihydrate phase and, indeed, indexing of X-ray Guinier camera patterns was also inconclusive, with respect to conclusive assignment of a space group.

The most recent comprehensive study [2], using Rietveld refinement of both X-ray and neutron powder data which was free from sample-dependent broadening, combined with careful control of the water vapor pressure during data acquisition, appears to have established definitive structures for both $\gamma$-$CaSO_4$ and the hemihydrate phase ($n = 0.5$), termed SH1. This work also established the structure of a further subhydrate with $n = 0.6$. In this latter case, however, there were ambiguities in the indexing process and further, since Fourier maps were inconclusive as to the sites of the water molecules, packing considerations were used to generate coordinates prior to Rietveld refinement. This is reflected in significant differences in oxygen coordinates generated using both X-ray and neutron techniques. This structure, SH2, must be regarded as tentative, at present. It is worth noting, also, the structure of an $n = 0.8$ phase (termed SH3) determined by single crystal methods [14], since this is the highest subhydrate yet reported in this system. However no hydrogen coordinates were reported, so the detail on the bonding of hydration waters to the framework must be regarded as less reliable.

The $\gamma$-$CaSO_4$ phase is built from chains of $CaO_8$ polyhedra linked by $SO_4$ tetrahedra. There are two types of chain, both of which run along the [001] direction, and which differ in the relative lengths of the Ca–O bonds within the $CaO_4$ plane and out of the plane [2]. The chain packing generates channels—two per unit cell—which run along the [001] direction, bounded by these linked chains. The space group is $C222$. The earlier study [15], with a smaller unit cell and $P6_222$ symmetry, constrained all chains to be equivalent.

On hydration, water molecules locate themselves within the channels. There have been discrepancies in the literature over whether the water molecules enter the coordination of the $Ca^{2+}$ ions [2] or are solely hydrogen bonded within the channels [15]. IR spectra of the hemihydrate have indicated two distinct sites (OW1 and OW2) which have been crystallographically verified [2,15]. The OW1 sites are located in special positions with the H atoms related by symmetry which makes both O–H bonds of equal length. In contrast, the OW2 sites are in general positions with distinct $H$ coordinates and differing bond lengths. In the SH1 (hemihydrate) structure, the water molecules enter the coordination shell of every second $Ca^{2+}$ ion in each chain and hydrogen bonds link the water molecules to sulfate oxygens in the chains. This ordering changes the space group from orthorhombic to monoclinic and doubles the $c$-axis of the unit cell. This arrangement results in six water molecules per unit cell, three in each channel. Within each channel the waters follow the sequence OW1–OW2–OW2 with each molecule spaced along the c-axis by $c/3$. Two other hydrates of $\gamma$-$CaSO_4$ which have been subject to structure determinations, are based on the same chain packing with different numbers and arrangements of water molecules. The water content of these was determined as $n = 0.60$ [2] (SH2) and $n = 0.8$ [14] (SH3). The space group of SH3 was given as trigonal with the $c$-axis halved and unit-cell volume a quarter of that found for SH1. Waters in SH2 and SH3 are located within more sites in each channel (four for SH2 and all six for SH3), than for SH1, but each site is only partially occupied (0.875 for SH2 and 0.81 for SH3), resulting in these overall hydration states.

The dehydration of gypsum has also been studied by other techniques [16] such as IR spectroscopy and thermogravimetry which tend to confirm $n = 0.5$ as the

Table 1
Crystallographic parameters for key phases

| Structure | SG | $a$ (Å) | $b$ (Å) | $c$ (Å) | $\beta$ | $Z$ | $V$ (Å$^3$) | Ref. |
|---|---|---|---|---|---|---|---|---|
| Gypsum | $I2/a$ | 5.679 | 15.202 | 6.522 | 118.43 | 4 | 495.2 | [11] |
| $\gamma$-$CaSO_4$ | $C222$ | 12.0777 | 6.9723 | 6.3040 | — | 6 | 530.86 | [2] |
| SH1 | $I121$ | 12.0317 | 6.9269 | 12.6712 | 90.27 | 12 | 1056.04 | [2] |

sole subhydrate phase. The crystallographic parameters for these key phases are given in Table 1.

It appears that, despite very many experimental attempts to investigate the crystallographic changes occurring on hydration of $\gamma$-$CaSO_4$, the only complete structure determination available (i.e., including experimentally derived $H$ positions) is that of the hemihydrate, SH1 [2].

## 3. Theory

Atomistic modelling of solids is based on the Born model, whereby interactions are categorized as either electrostatic (long range) or short range, and are described by simple analytical functions. The Coulomb energies are summed by the Ewald method [17] and the short-range interactions are built from a variety of functional forms empirically appropriate to particular atoms or ions and which describe both attractive (dispersive) and repulsive components. For solids including molecular ion species [18], distinct intramolecular potentials need to be provided, in addition to the inter-atomic interactions. A further refinement, needed here, is the introduction of polarizability to accurately describe the oxygen atom in the water molecule [19]. This is achieved by the shell model [20] approach in which the ion is modelled as massive, positive core coupled to a massless, negative shell by a harmonic spring potential. The net ionic charge remains fixed. The polarizability, linked to the core—shell displacement, can therefore vary with the local environment. The shell model for oxygen has also been used in simulations involving the carbonate ion [21] but has not found to be relevant, to date, in studies on sulfates.

In this work the following functional forms were used to represent potential energy functions:

The Buckingham potential:

$$U_{ij}(r) = A_{ij}\exp\left(\frac{-r}{\rho_{ij}}\right) - C_{ij}r^{-6}$$

used to represent short-range interactions between atoms $i$ and $j$. The Morse potential which successfully models the intra-atomic interactions within molecular ions:

$$U_{ij}(r) = D_{ij}[\{1-\exp[-\beta_{ij}(r-r_{oij})]^2 - 1\}].$$

The Lennard-Jones (12–6) function which is also appropriate to inter-atomic interactions; here used to model the interactions between the $O$ atoms in water molecules

$$U_{ij}(r) = A_{ij}r^{-12} - B_{ij}r^{-6}.$$

The three-body forces within the $SO_4^{2-}$ ions and within the water molecules, are modelled by a spring potential

$$U_{ij}(r) = \tfrac{1}{2}k_\theta(\theta-\theta_0)^2.$$

In a similar fashion the shell model potential for the oxygen atoms, in the water molecules, are parameterized through a simple harmonic potential

$$U_{ij}(r) = \tfrac{1}{2}k_s(r-r_0)^2.$$

All calculations have been carried out using the general lattice utility program (GULP) [22] provided by Julian Gale and running on a Silicon Graphics Workstation under UNIX. This approach uses lattice symmetry, together with analytical first and second derivative and Newton–Raphson methods, to minimize lattice energy in a computationally efficient fashion. The program may be used both to calculate structures and properties from a given set of potentials and to derive potentials using structure and properties information, such as elastic or dielectric constants, provided by the user. In the latter mode, a strategy of optimizing the structure during the fit, thereby using structural displacements to drive the fitting process rather than simply going for minimizing the forces on each atom, provides a better quality of fit.

Many sets of transferable potentials are now available in the literature and some have been used in this work. A set of potentials appropriate for modelling the bulk and surface properties of the alkali metal and alkaline earth sulfates (including $\beta$-$CaSO_4$) have been derived through fitting to crystal structures and elastic properties [7]. Molecular dynamics studies on the interaction of water with MgO surfaces led to the development of a shell-model potential set for the water molecule appropriate to its behavior in inorganic systems [19]. The majority of the functions needed for this present work are therefore available from these two sources. However, potentials for the interaction of the water molecule with the $Ca^{2+}$ and $SO_4^{2-}$ ions were not available and have been derived by similar fitting methods. All these potential functions are summarized in Table 2.

Table 2
Potential functions used in this work

| Bond | Type | $A$ (eV) | $\rho$ (Å) | $C$ (eV Å$^6$) | Cut off (Å) | Ref. |
|---|---|---|---|---|---|---|
| Ca–O | Buck | 1651.35 | 0.2931 | 0 | 20 | [7] |
| Ca–$O_{ws}$ | Buck | 1597.08 | 0.29213 | 0 | 20 | This work |
| O–$O_{ws}$ | Buck | 57143.20 | 0.22425 | 75.7016 | 20 | This work |
| H–O | Buck | 2481.27 | 0.05978 | 0 | 20 | This work |
| O–O | Buck | 103585.02 | 0.200 | 25.93 | 15 | [7] |
| H–$O_{ws}$ | Buck | 396.2700 | 0.2500 | 10.00 | 20 | [19] |
| Bond | Type | $k$ (eV Å$^{-2}$) | | | Cut off (Å) | Ref. |
| $O_{wc}$–$O_{ws}$ | Spring | 209.45 | | | 0.8 | [19] |
| Bond | Type | $D$ (eV) | $\beta$ (Å$^{-1}$) | $r_0$ (Å) | Cut off (Å) | Ref. |
| H–$O_{ws}$ | Intra-Morse | 6.2037 | 2.2200 | 0.924 | 1.1 | [19] |
| O–S | Intra-Morse | 5.000 | 1.2000 | 1.5050 | 1.8 | [7] |
| Bond | Type | $A$ (eV Å$^{12}$) | $B$ (eV Å$^6$) | | Cut off (Å) | Ref. |
| $O_{ws}$–$O_{ws}$ | Lenn 12 | 39344.98 | 42.15 | — | 40 | [19] |
| Bond | Type | $k$ (eV rad$^{-2}$) | $\theta_0$ | | Cut off (Å) | Ref. |
| O–S–O | Harm three body | 15.0000 | 109.47° | — | 1.8 1.8 3.2 | [7] |
| H–$O_w$–H | Harm three body | 4.1998 | 108.69° | — | 1.2 1.2 2.4 | [19] |

*Note:* An "s" subscript indicates a potential with the oxygen shell whereas a "c" subscript indicates the core.

Table 3
Comparison of experimental and computed crystallographic parameters for $\gamma$-$CaSO_4$

| Space group | $\gamma$-$CaSO_4$ | | | | |
|---|---|---|---|---|---|
| | Experiment [2] *C*222 | Simulation *C*222 | Experiment [15] $P6_222$ | Simulation $P6_222$ | Simulation *P*1 |
| $a$ (Å) | *12.0777* | 12.0774 (0.00%) | *6.9694* | 6.9772 (0.05%) | 12.0772 (0.00%) |
| $b$ (Å) | *6.9723* | 6.9728 (0.01%) | *6.9694* | 6.9772 (0.05%) | 6.9728 (0.01%) |
| $c$ (Å) | *6.3040* | 6.4133 (1.73%) | *6.3033* | 6.4207 (1.74%) | 12.8267 (1.73%) |
| $\beta$ | — | — | *120* | 120 | 90.00 |
| $V$ (Å$^3$) | *530.86* | 540.084 (+1.74%) | *265.149* | 270.045 (+1.85%) | 1080.16 (1.74%) |
| Ca–O (Å) | *2.356–2.588* | 2.384, 2.634 | — | 2.384, 2.634 | 2.384, 2.634 |
| S–O (Å) | *1.48–1.49* | 1.446 | — | 1.446 | 1.446 |

*Note:* The simulation of $\beta$-$CaSO_4$ [7], using the same potential set, gave the following comparisons between the computed and experimental unit cell: $a$: −1.39%, $b$: +1.39%, $c$: +0.33%, $V$: +0.003%.

## 4. Derivation of potentials and results for known structures

The results of atomistic simulations of $\gamma$-$CaSO_4$, together with the derivation of new potentials needed for the study of hydrated $CaSO_4$ phases, are given here. Using this potential set, its transferability to $CaSO_4 \cdot 2H_2O$ and to $CaSO_4 \cdot 0.5H_2O$, the structures of which are known, is evaluated.

The structure of $\beta$-$CaSO_4$ (insoluble anhydrite) was modelled previously [7] using the potentials given in Table 2, with some success. Interest in the hydrates of $CaSO_4$ means that transferring this potential set to the simulation of $\gamma$-$CaSO_4$ (soluble anhydrite) is important. The results of this are given in Table 3. The two space groups proposed experimentally for this structure have been examined, together with a supercell approach where the $c$-axis is doubled and all symmetry operations removed to create a unit cell the same size as that for the SH1 subhydrate. In this latter case, the unit-cell parameters and atomic coordinates for the SH1 framework atoms were used as initial parameters. In all cases,

the crystallographic parameters are very well reproduced, with the largest discrepancy occurring for the crystallographic *c*-axis (+1.74%). Bond length agreement is also very satisfactory. All three simulations result in basically the same structure with the atom positions in the supercell simulation revealing the true higher symmetry of *C*222. It is reassuring that, by starting with a dehydrated SH1, we can generate the higher symmetry of the $\gamma$-$CaSO_4$ structure.

Having successfully modelled the anhydrous phases, attention was then given to simulating the known hydrates of $CaSO_4$, using the structure and properties of gypsum to generate additional potentials for water molecule interactions. New potentials for the interactions between $Ca^{2+}$ and $SO_4^{2-}$ with $H_2O$ were determined by fitting to the crystal structure [11], elastic constants [23] and selected IR frequencies [16] for gypsum ($CaSO_4 \cdot 2H_2O$). As IR spectroscopy has been used extensively to characterize the hydration of gypsum, e.g., [16], both the O–H…O stretching (around 3500 $cm^{-1}$) and bending (around 1600 $cm^{-1}$) spectra have been used here to validate the simulations. The Buckingham parameters derived from this process are given in Table 2. The consequent results of modelling both the structure and properties for this system are given in Tables 4 and 5.

It is important that the simulation accurately predicts not only the unit-cell parameters but also key bond lengths and angles in the structure itself. In this instance, attention must be paid to the hydrogen bond parameters predicted by the calculations. It is clear from these results that the unit cell is very close to experiment indeed, with the exception of the **a** dimension which, although underestimated by 1.55%, is nevertheless satisfactory. As a consequence the volume is underestimated by a similar amount. All bond lengths are fairly well predicted, though simulation slightly overestimates both the $Ca–O_{water}$ and the O–H…O distances. Agreement with both the hydrogen bond bend and stretch IR frequencies are good. Comparison of experimental elastic constants with those predicted is reasonable though there are minor discrepancies (Table 5).

As a additional test and as preparation for further modelling of hydration in $CaSO_4$, this full potential set was used to model the experimentally determined crystal structures of the $CaSO_4$ subhydrate phases, described previously. These are the well-specified SH1 hemihydrate and the less reliable SH2 ($n = 0.6$) and SH3 ($n = 0.8$) structures. In the latter case, coordinates for the hydrogen positions within the water molecule were estimated, using geometrical considerations, prior to using GULP. The results of this are given in Table 6. In the case of SH1 and SH3 the calculations were repeated with all symmetry operations within unit cell removed (*P*1 space group).

The simulation of the SH1 phase is excellent in terms of the unit-cell parameters, Ca–O bond lengths and the hydration water IR frequencies. Although the $Ca–O_w$ and O–H…O bond lengths are shorter than found experimentally and simulation does not predict the full range of values found experimentally, the $O_w$…O distances are very close to experiment. This is due to the hydrogen bond angle, at around 155°, being on the low side. However given the simplicity of the interatomic potential functions used, with no provision for angular dependency in the hydrogen bond itself, agreement overall is quite acceptable. Agreement with the IR frequencies, where they are available, is fairly good. The simulations for SH2 and SH3 compare less well with experiment, with the unit-cell dimensions being consistently on the large side and differences, as well, in the distances associated with the water molecules. However as the $Ca–O_w$ bond lengths are on the large side for SH2 but on the low side for SH3, some of this discrepancy may reflect acknowledged uncertainties in the experimental data for these two systems. It is worth

Table 4
Comparison of experimental and computed crystallographic parameters for $CaSO_4 \cdot 2H_2O$ (gypsum)

| Space group | $CaSO_4 \cdot 2H_2O$ | |
|---|---|---|
| | Experiment *I*12/*c*1 | Simulation *I*12/*c*1 |
| *a* (Å) | 5.679 | 5.591 (−1.55%) |
| *b* (Å) | 15.202 | 15.234 (0.21%) |
| *c* (Å) | 6.522 | 6.526 (0.06%) |
| $\beta$ | 118.43 | 118.428 (0.00%) |
| *V* (Å$^3$) | 495.2 | 488.788 (−1.29%) |
| Ca–O (Å) | 2.546, 2.552, 2.366 | 2.671, 2.458, 2.336 |
| $Ca–O_w$ (Å) | 2.374 | 2.425 |
| S–O (Å) | 1.471, 1.474 | 1.440, 1.449 |
| O–H…O (Å) | 1.856, 1.941 | 1.883, 1.890 |
| $O…O_w$ (Å) | 2.807, 2.882 | 2.820, 2.834 |
| IR ($cm^{-1}$) | 3550, 3400 [16] | 3568, 3422, 3437 |
| IR ($cm^{-1}$) | 1690, 1610 [16] | 1752, 1692 |

Table 5
Comparison of experimental and computed elastic constants for gypsum

| (× 10 GPa) | $C_{11}$ | $C_{22}$ | $C_{33}$ | $C_{44}$ | $C_{55}$ | $C_{66}$ | $C_{12}$ | $C_{13}$ | $C_{15}$ | $C_{23}$ | $C_{25}$ | $C_{35}$ | $C_{46}$ |
|---|---|---|---|---|---|---|---|---|---|---|---|---|---|
| Computed | 10.13 | 9.81 | 7.90 | 0.87 | 3.12 | 1.072 | 5.09 | 2.96 | 1.01 | 2.97 | −0.74 | 2.60 | 0.12 |
| Experimental [23] | 7.86 | 6.27 | 7.26 | 0.91 | 2.64 | 1.04 | 4.10 | 2.69 | −0.70 | 2.42 | 0.31 | −1.74 | −0.16 |

Table 6
Computed and experimental crystallographic parameters for $CaSO_4 \cdot nH_2O$

| Space group | System | | | | | | | |
|---|---|---|---|---|---|---|---|---|
| | Experiment 0.5 $H_2O$ (SH1) *I121* | Simulation (SH1) *I121* | Simulation (SH1) *P*1 | Experiment 0.6 $H_2O$ (SH2) *I121* | Simulation (SH2) *I*121 | Experiment 0.8 $H_2O$ (SH3) $P3_121$ | Simulation (SH3) $P3_121$ | Simulation (SH3) $P1^*$ |
| *a* (Å) | 12.0317 | 12.0202 (−0.10%) | 12.0174 (−0.12%) | 11.9845 | 11.9659 (−0.16%) | 6.968 | 7.067 (+1.4%) | 7.026 (+0.8%) |
| *b* (Å) | 6.9269 | 6.9200 (−0.10%) | 6.9228 (−0.06%) | 6.9292 | 6.9761 (+0.68%) | 6.968 | 7.067 (+1.4%) | 7.026 (+0.8%) |
| *c* (Å) | 12.6712 | 12.7961 (+0.99%) | 12.7951 (+0.98%) | 12.7505 | 12.8666 (+0.91%) | 6.410 | 6.5403 (+2.03%) | 6.572 (+2.5%) |
| *β* | 90.27 | 90.608 (+0.37%) | 90.552 (+0.31%) | 90.00 | 91.916 (2.13%) | — | — | — |
| *V* (Å$^3$) | 1056.04 | 1064.32 (+0.78%) | 1064.44 (+0.80%) | 1058.84 | 1073.440 (+1.38%) | 269.53 | 282.847 (+4.95%) | 280.970 (+4.2%) |
| Ca–O (Å) | 2.400–2.688, 2.930 | 2.378–2.783, 2.929 | 2.361–2.798, 2.940 | 2.199–2.846, 3.059 | 2.364–2.750, 2.844 | 2.454–2.657 | 2.422–2.628, 2.887 | 2.372–2.739 |
| Ca–$O_w$ (Å) | 2.365, 2.419 | 2.462, 2.474 | 2.464, 2.469 | 2.262–2.617 | 2.590, 2.594 | 2.59 | 2.377 | 2.405 |
| S–O (Å) | 1.480–1.509 | 1.44–1.45 | 1.44–1.45 | 1.452–1.557 | 1.437–1.451 | 1.442, 1.468 | 1.439, 1.454 | 1.439–1.460 |
| O–H…O (Å) | 2.17–2.34 | 2.083–2.107 | 2.058–2.168 | 2.11–2.69 | 1.974–2.180 | — | 2.303 | 2.265–2.324 |
| O…$O_w$ (Å) | 2.85–3.03 | 2.885–2.907 | 2.884–2.907 | 2.85–2.96 | 2.875–2.968 | 2.73–3.26 | 2.808, 2.989, 3.142 | 2.988–3.055 |
| IR (cm$^{-1}$) | 1622 [16] | 1672, 1675, 1680 | 1672, 1678, 1683 | NA | 1469, 1484 | NA | 1350 | 1358 |
| IR (cm$^{-1}$) | 3552, 3620 [16] | 3499, 3645 | 3496, 3642 | NA | 3271, 3383 | NA | 3145, 3234 | 3142, 3236 |

*Note*: 2.400–2.688 indicates a range of bond lengths; 2.930 or 1.442, 1.468 indicate individual bond lengths.

noting that the simulated IR frequencies for both SH2 and SH3 are distinctly different from those for SH1 but that no experimental data is available to confirm this.

## 5. Simulations of the hydration of γ-$CaSO_4$

Using this validated potential set, the water–matrix interactions were studied in greater detail using the anhydrous γ-$CaSO_4$ structure (set up in the *P*1 space group) as the matrix. The initial task was to use the *translate* option within GULP to identify stable bonding locations for a water molecule within the channels and the consequent effect on the matrix of the presence of each occupied site. A water molecule was positioned within one of the two channels in the unit cell (labelled A and B for convenience), the structure optimized, then the molecule was advanced a short distance along the channel and the process repeated until the full *c*-axis repeat had been traversed. The other channel was left empty thus effectively isolating the walls of the occupied channel, to some extent from external influence.

There are twelve unique $Ca^{2+}$ ions in each unit cell, of which two (Ca1 at $z = 0.5$ and Ca11 at $z = 0.0$) are shared between adjacent A channels and two (Ca2 at $z = 0.0$ and Ca12 at $z = 0.5$) between B channels. The remaining eight are shared between adjacent channels of different labels (A and B). These cations have been numerically labelled as shown in Fig. 1. Within each channel the $Ca^{2+}$ ions are approximately equi-spaced along the *c*-axis, separated by a distance of $\sim c/6$ and positioned in pairs, at opposite corners of the hexagonal channel cross-section. The sites can be viewed as two spiral paths each of six ions, but 180° out of phase, running up each channel. Within the structures determined experimentally, where the space group symmetry is higher than P1, the number of unique $Ca^{2+}$ ions is reduced—to four for SH1 and SH2 and one for SH3.

Twelve sites for each channel within the unit cell were identified where the oxygen water ($O_w$) enters the $Ca^{2+}$ coordination shell and hydrogen bonding links the molecule to sulfate oxygens on the channel walls. This evidence supports the crystal structures experimentally determined by Bezou [2]. All sites are energetically equivalent and occupancy alters the structure of the matrix in distinct ways, depending on whether the site is shared between crystallographically identical channels. The results for these two types of site in channel A and comparison with the anhydrous cell, are summarized in Table 7.

It is clear that the presence of a single hydration water both reduces the unit-cell symmetry from orthorhombic to either monoclinic or triclinic, depending on the occupation site, and also causes the cell volume to contract significantly. In the monoclinic case, the water is less tightly held within the Ca coordination and the

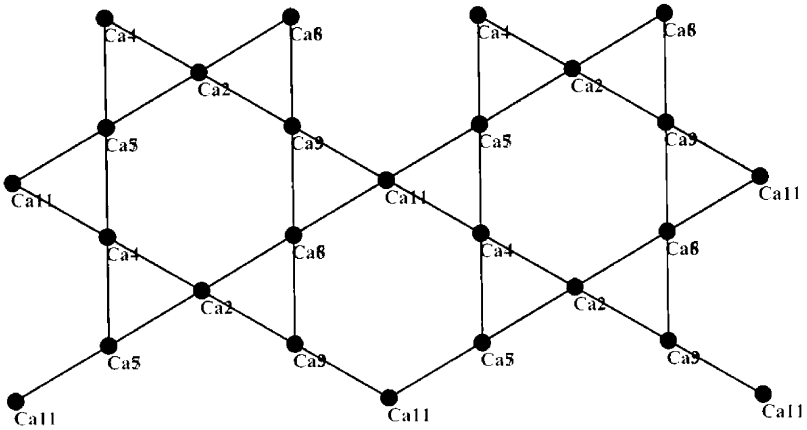


Fig. 1. The framework of $Ca^{2+}$ ions in calcium sulfate hemihydrate, viewed along the (001) axis, showing the 'A' and 'B' channels.

Table 7
Matrix interactions with a single water in one channel (A)

| $U$ (eV/uc) | $H_2O$ binding energy (eV) | $Ca^{2+}$ site | System | Unit-cell volume (Å$^3$) | Ca–$O_w$ (Å) | H–O (Å) | $O_w$–O (Å) | $O_w$–H–O angle | IR ($cm^{-1}$) |
|---|---|---|---|---|---|---|---|---|---|
| −567.794 | — | None | O | 1080.16 | — | — | — | — | — |
| −581.048 | −0.847 | 1,11 | M | 1077.34 | 2.754 | 2.065 | 2.928 | 155° | 3664 |
| | | | | | | 2.065 | 2.928 | 155° | 3513 |
| | | | | | | | | | 1682 |
| −581.048 | −0.847 | All others | T | 1076.38 | 2.668 | 2.029 | 2.890 | 154° | 3669 |
| | | | | | | 2.146 | 3.004 | 153° | 3514 |
| | | | | | | | | | 1688 |

*Note:* O: orthorhombic, M: monoclinic, T: triclinic.

hydrogen bonds are symmetric. In the triclinic case, the water is closer to the $Ca^{2+}$ site but the hydrogen bonds are asymmetric, with one hydrogen bonding more strongly than the other. These lead to the same lattice energy for each. This work confirms the existence of two distinct sites which agrees with the crystallographic investigation of SH1 [2]. $Ca^{2+}$ sites labelled 1 and 11 in channel A and sites 2 and 12 in channel B, correspond to OW1 locations while all others correspond to OW2. However, the simulated IR spectra are almost identical. Indeed, these simulations show that the splitting into two stretching frequencies, believed to be indicative of two sites, can be explained through a single, bound water molecule.

The change in lattice energy consequent on the bonding of a single water molecule within a channel, may be estimated from the difference in lattice energy between the anhydrous and hydrated systems, less the intra-molecular energy of the water molecule itself (twice the well depth for the $O_w$–H Morse potential). This resulting value comprises, not only the actual bonding to the matrix, but also changes within the matrix itself and minor strains within the molecule. It is instructive to compare this with the activation energy for dehydration of $CaSO_4 \cdot 0.5H_2O$ measured by thermogravimetric techniques [16]. There are variations in the literature depending on the water vapor pressure used during measurement, but a value around $-90.3\,kJ\,mol^{-1}$ is commonly obtained [16]. This is equivalent to $-0.938\,eV$ per $H_2O$, very close to the binding energy calculated in the table. It should be noted, for the moment, that this experimental value is an average for dehydration of all six water molecules within the unit cell. If this calculation is carried out for the simulated structure of SH1, shown in Table 6, a value of $-1.078\,eV$ per $H_2O$ is obtained.

Configurations of two water molecules within a single channel were then investigated. Symmetry considerations show that many are equivalent. There are, in total, 10 distinct arrangements possible for bonding two waters in a channel. The binding energy per molecule was calculated in the same fashion as previously. These data are summarized in Table 8.

This table reveals many interesting features. Firstly, configurations where the two molecules are directly opposite each other or adjacent but separated by $c/3$ do not converge, reflecting rejection of these arrangements simply on space-filling grounds. For the majority of configurations that converge, the crystal system symmetry is strongly affected by the occupied bonding sites, with triclinic, monoclinic and orthorhombic possibilities caused by distortion of the channel framework. There is also very significant variation in the unit-cell volume and, indeed, the lattice energy as well. This latter

Table 8
Summary of simulations with two waters in one channel (A)

| Water bonding sites labelled by the appropriate Ca atom number | Crystal System | $U$ (eV/uc) | $H_2O$ bonding energy per molecule (eV) | Cell volume (Å$^3$) | Ca–$O_w$ bond lengths (Å) | Bond status |
|---|---|---|---|---|---|---|
| 1+11 | M | −594.365 | −0.878 | 1073.81 | 2.684+2.684 | Bound |
| | O | −594.153 | −0.772 | 1082.96 | 2.925+2.925 | Adsorbed |
| 5+7, 6+8, 3+9, 4+10 | T | −594.371 | −0.881 | 1072.73 | 2.625+2.625 | Bound |
| 6+7, 5+8, 3+10, 4+9 | | | | | No convergence | |
| 6+5, 7+8, 3+4, 9+10 | T | −594.243 | −0.817 | 1077.04 | 2.679+2.679 | Bound |
| 3+6, 8+9, 7+10, 4+5 | M | −594.011 | −0.701 | 1085.32 | 3.189+3.189 | Adsorbed |
| 6+9, 3+8, 4+7, 5+10 | | | | | No convergence | |
| 11+3, 1+4, 1+6, 11+5 | T | −594.359 | −0.875 | 1073.04 | 2.656+2.656 | Bound |
| 1+9, 1+7, 11+8, 11+10 | T | −594.074 | −0.732 | 1084.72 | 3.203+3.203 | Adsorbed |
| 11+7, 1+8, 1+10, 11+9 | T | −594.400 | −0.896 | 1072.61 | 2.618+2.675 | Bound |
| 1+3, 1+5, 11+6, 11+4 | T | −594.157 | −0.774 | 1081.37 | 2.778+3.030 | Adsorbed |
| 6+10, 4+8, 7+3, 5+9 | M | −594.370 | −0.880 | 1075.18 | 2.663+2.663 | Bound |
| 8+10, 4+6, 3+5, 7+9 | M | −594.363 | −0.877 | 1072.16 | 2.668+2.668 | Bound |

quantity reflects differences in the binding energies of the water molecules among configurations. Most importantly, there are now two types of site occupation indicated by the Ca–$O_w$ bond lengths calculated for these configurations. "Short" bond lengths of around 2.61–2.68 Å indicate that the water molecule is held within the $Ca^{2+}$ coordination shell, in a similar fashion to the results found previously for a single molecule. These correspond to a mean binding energy per molecule of −0.872 eV. Several of these configurations contract the unit cell further than was the case for a single hydration water. However, configurations where the bond length is significantly longer—around 2.8–3.2 Å—correspond to the oxygen of the water molecule being outside this coordination, with the sole bonding to the framework being hydrogen bonds to sulfate oxygens. These are termed "adsorbed" sites in the table. The mean bonding energy per molecule for these is substantially lower, at −0.745 eV. Examination of the water molecule coordinates in these cases reveals that the adsorbed waters are positioned in the center of the channel, rather than towards a particular $Ca^{2+}$ ion. Such adsorbed waters do not contract the unit-cell volume but, in fact, drive a small expansion, as shown by the figures in the table (recall that the simulated anhydrous cell volume is 1080.16 Å$^3$). Configurations involving sites 1 and 11 allow both bound and adsorbed configurations. By examining the difference in lattice energy between these, we can estimate the increase in binding energy consequent on entering the $Ca^{2+}$ coordination shell. A maximum value of around −0.143 eV is indicated for sites such as 11+3. This represents around 16% of the total binding energy for a bound water molecule. Note that almost all these bound sites have a larger binding energy than found for a single molecule. The lowest energy configuration for a pair of

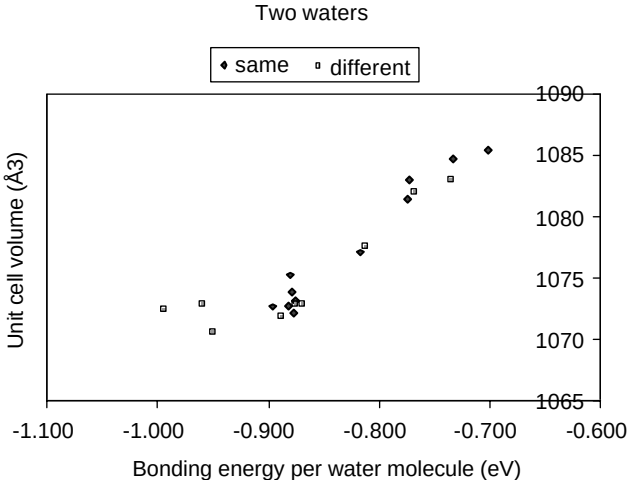


Fig. 2. Unit-cell volume versus bonding energy per molecule for two waters distributed between the two channels in the unit cell.

water molecules within a single channel has an energy of −0.896 eV per molecule and corresponds to occupation of an OW1 and an OW2 site, separated by a distance of approximately $c/3$. This corresponds to one of the smallest unit-cell volumes. Most bound pairs are in configurations where the molecules are separated by $c/2$.

The link between bonding energy and both unit-cell volume and Ca–$O_w$ bond length may be explored graphically in Figs. 2 and 3. Data points corresponding to the two water molecules being in the same channel or in different channels (A and B) are shown using different symbols. Both graphs show fairly smooth monotonic variation between the variables. The strongest bonding energy corresponds to waters held within the $Ca^{2+}$ coordination sphere and with a consequent minimum unit-cell volume. All bound configurations have similar

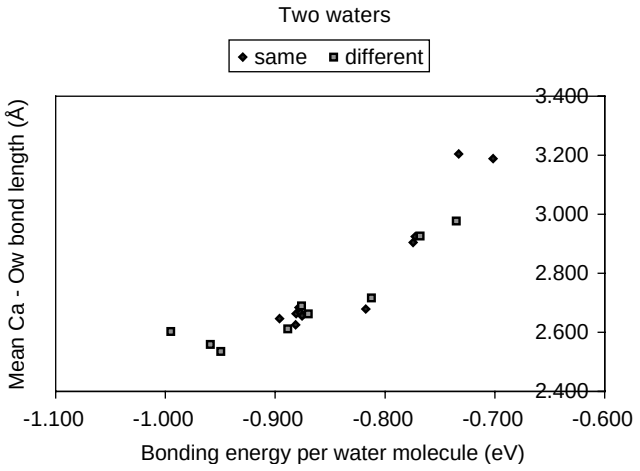


Fig. 3. Mean Ca–$O_w$ bond length versus bonding energy per molecule for two waters distributed between the two channels in the unit cell.

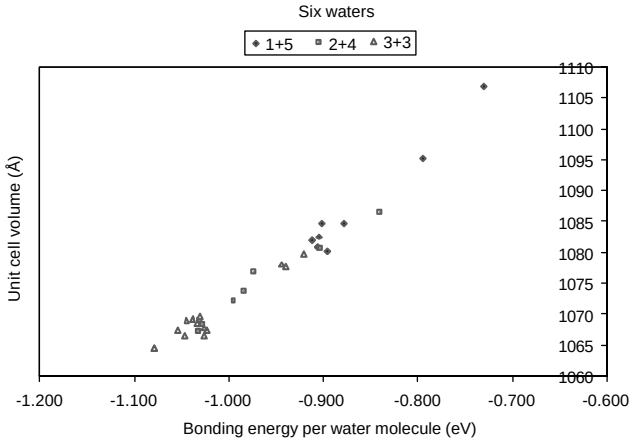


Fig. 4. Unit-cell volume versus bonding energy per molecule for six waters distributed between the two channels in the unit cell.

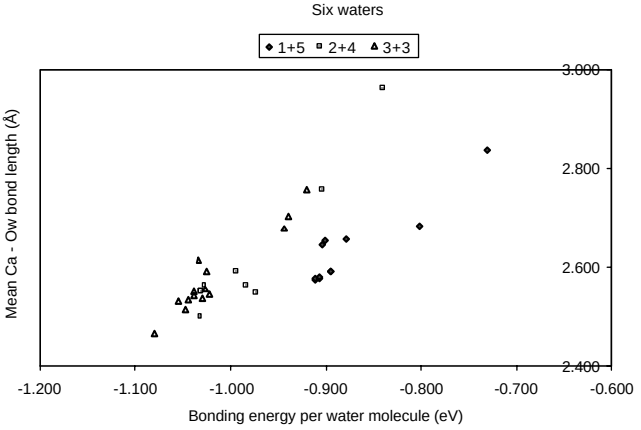


Fig. 5. Mean Ca–$O_w$ bond length versus bonding energy per molecule for six waters distributed between the two channels in the unit cell.

Ca–$O_w$ bond lengths but a range of binding energies. The trend that is emerging from these calculations is that as water molecules are bound in the channels they pull the framework inwards producing a volume contraction. If they are merely adsorbed, there is a net repulsion causing expansion of the unit cell. Some of the simulations that have been carried out with the two waters placed in adjacent channels show slightly higher binding energies than for single channel occupation. Clearly, contraction of the unit cell cannot continue indefinitely, so modelling with larger numbers of water molecules is needed to investigate this effect.

Calculations have been carried out with a fixed number of water molecules assigned to the unit cell, ranging from three to eight. These were arranged between the channels in all possible ratios and, within each channel, many configurations (up to 40 in some cases) were sampled both randomly and including those most likely to be favored on space-filling grounds. This has yielded a wealth of data on hydration configurations including bonded and adsorbed water molecules.

All sets of data produced graphs showing trends similar to those shown for two molecules in the unit cell. In all cases the plot of unit-cell volume versus bonding energy exhibited a clear trend line, usually with a fairly linear region, with a high density of configurations corresponding to minimum energy and corresponding minimum unit-cell volume. Some configurations have a volume larger than for the anhydrous cell; this results from a high proportion of adsorbed rather than bound waters in the channels. As the number of waters increases the average Ca–$O_w$ bond lengths become smaller, indicating that the hydration waters were being drawn more tightly into the $Ca^{2+}$ coordination shell. Figs. 4 and 5 show typical graphs, for six water molecules per unit cell (the $n = 6$ case is the hemihydrate). The distribution of waters between the channels, e.g., 5 + 1, 4 + 2, or 3 + 3, is shown by the symbols. There is a fairly linear correlation with the low energy end favoring equally apportioned hydration (3 + 3) while the upper end, indicating mainly adsorbed waters, corresponding to the ratio of 5 + 1. The mean bond length variation conceals the fact that for many configurations including adsorbed sites there is a significant variation of bond lengths around the mean. The most tightly bound configurations correspond to the smallest unit-cell volumes.

Plots both of average $Ca^{2+}$–$O_w$ bond length and of unit-cell volume, versus bonding energy per water molecule, including data for all configurations studied, are shown in Figs. 6 and 7. These provide converging evidence of the structural and energetic changes taking place as the hydration level of the $CaSO_4$ crystal is altered. Both graphs show, as a general trend, an increase in the magnitude of the bonding energy of the water molecules as the hydration level in the crystal increases. This reaches a maximum in the region of five to six $H_2O$ per unit cell. Higher levels of hydration cause

the unit cell to expand thereby increasing the $Ca^{2+}$–$O_w$ bond length and decreasing the bonding energy. This "loop" in the graphical trend is most clearly seen in the unit-cell dependency (Fig. 5). This could explain why the $CaSO_4 \cdot nH_2O$ structures which have been determined experimentally, had $n \sim 0.5$ and hydration levels significantly lower or higher than this have not been found. The predication, through these modelling studies, of the existence of a range of energetically favorable configurations in the approximate range 5–7 $H_2O$ per unit cell also shows why experimental structures have been found close to, but not exactly at, the hemihydrate stoichiometry. The link between unit-cell volume and hydration is of great interest and suggests that careful experimental measurement of this parameter could provide a measure of $n$ in both transient and thermodynamically stable $CaSO_4 \cdot nH_2O$. There is of course some limited data available on this from the X-ray structural studies referred to already in this paper. There are four structures for which both $n$ and the unit-cell parameters are provided (Tables 3 and 6). These experimental and modelling data are presented together in Table 9. Leaving aside the general comparisons between absolute values which have been discussed previously, it is clear that the experimental trends in expansion and contraction in the unit cell are predicted by the atomistic modelling techniques. The simulation tends to overestimate these effects by a factor of about 2.5 but otherwise this provides good evidence that the theoretical predictions are borne out by the available experimental data.

Finally, it is worth noting that these calculations show that the configuration with the most tightly bound water molecules corresponds to the SH1 structure determined by Bezou et al [2].

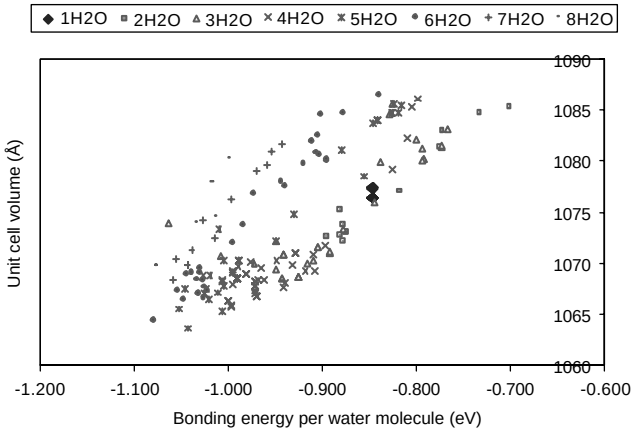


Fig. 6. Unit-cell volume versus bonding energy per molecule for all hydration configurations studied, from $1H_2O$ to $8H_2O$ per unit cell.

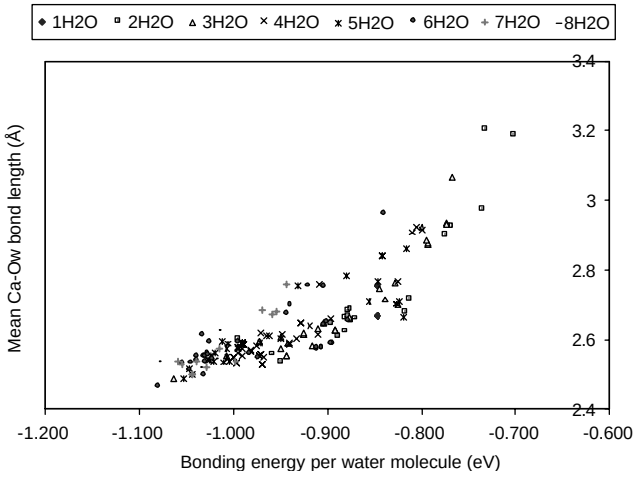


Fig. 7. Mean Ca–$O_w$ bond length versus bonding energy per molecule for all hydration configurations studied, from $1H_2O$ to $8H_2O$ per unit cell.

## 6. Conclusions

This work has shown that the hydration properties of $CaSO_4 \cdot nH_2O$ may be modelled using atomistic methods and empirical potentials, many transferred from the literature. Using the structure and properties of $CaSO_4 \cdot 2H_2O$ (gypsum), additional potentials, describing the interactions of water with $Ca^{2+}$ and $SO_4^{2-}$ ions, have been derived. This complete potential set has been shown to predict successfully the crystal structures of anhydrous $\gamma$-$CaSO_4$ and some of the $CaSO_4 \cdot nH_2O$

Table 9
Relationship between $nH_2O$ and unit-cell volume, for modelling and experiment

| $n$ | Unit-cell volume (expt) (Å$^3$) | Unit-cell volume (theory) (Å$^3$) | Change in cell volume from ($\gamma$-$CaSO_4$ (%) (expt.) | Change in cell volume from ($\gamma$-$CaSO_4$ (%) (theory) |
|---|---|---|---|---|
| 0 ($\gamma$-$CaSO_4$) | 1061.72[a] | 1080.16[a] | — | — |
| 0.5 | 1056.04 | 1064.44 | −0.54% | −1.46% |
| 0.6 | 1058.84 | 1073.44 | −0.27% | −0.62% |
| 0.8 | 1078.12[b] | 1123.89[b] | +1.54% | +4.05% |

[a] Scaled by ×2 for direct comparison.
[b] Scaled by ×4 for direct comparison.

phases for which structures of reasonable quality have been experimentally determined. Using the structure of $\gamma$-$CaSO_4$ as a matrix, a series of detailed calculations were carried out to investigate the bonding sites, energies and molecular configurations within the unit cell for varying numbers of water molecules. For a single molecule, bonding sites within the coordination of every $Ca^{2+}$ ion on the walls of the hydration channels, were discovered. The sensitivity of the matrix to the inclusion of hydration molecules was demonstrated by the consequent changes to both the unit-cell symmetry and volume. For two water molecules within a channel, modelling predicted the existence of two types of site: one bound within the $Ca^{2+}$ coordination sphere and hydrogen bonded to matrix $SO_4^{2-}$ ions, the other, named an adsorbed site, situated in the center of the channel and relying wholly on hydrogen bond interactions. The unit-cell volume, in particular, was found to be very sensitive to the configuration adopted by the pair of hydration molecules. Occupation of bound sites compresses the cell volume while occupation of adsorbed sites tends to expand it, above the value calculated for anhydrous $\gamma$-$CaSO_4$. Estimates of the average bonding energy per molecule were found to be in good agreement with activation energies measured experimentally by thermogravimetric techniques. Further modelling, for larger numbers of waters across a wide range of configurations, revealed a strong correlation between the average bonding energy, the average $Ca^{2+}$–$O_w$ coordination distance and the unit-cell volume. The most stable configurations, as measured by these parameters, were predicted to be for values of around 5–7 $H_2O$ molecules per unit cell with the single, most strongly bound, arrangement of waters being the hemihydrate phase SH1 reported by Bezou et al. [2]. The prediction that these most stable phases would be characterized by a minimum in the unit-cell volume was shown to be supported by the limited range of specific experimental data available. It is proposed that further experimental high-resolution XRD studies, over a wide range of known hydration conditions, need to be done in order to test these predictions thoroughly.

## Acknowledgments

I am grateful to Dr. Rob Jackson for advice and guidance with the GULP program and for the provision of computing facilities. I wish to thank Dr. Julian Gale for supplying the GULP code at Keele.

## References

[1] A.J. Lewry, J. Williamson, J. Mater. Sci. 29 (1994) 5279–5284.
[2] C. Bezou, A. Nonat, J.-C. Mutin, A. Norlund Christensen, M.S. Lehmann, J. Solid. State Chem. 117 (1995) 165–176 DOI 10.1006/jssc.1995.1260.
[3] W. Abriel, K. Reisdorf, J. Pannetier, J. Solid. State Chem. 85 (1990) 23–30.
[4] C. Solberg, S. Hansen, Cement Concrete Res. 31 (2001) 641–646 DOI 10.1016/S0008-8846(01)00464-1.
[5] E. Badens, S. Veesler, R. Biostelle, J. Crystal Growth. 198/199 (1999) 704–709 doi: 10.1016/S0022-0248(98)01206-8.
[6] D. Freyer, G. Reck, M. Bremer, W. Voigt, Monatsh. Chem. 130 (10) (1999) 1179–1193.
[7] N.L. Allan, A.L. Rohl, D.H. Gay, R.A. Catlow, R.J. Davey, W.C. Mackrodt, Faraday Discuss. 95 (1993) 273–280.
[8] N.H. de Leeuw, S.C. Parker, J. Chem. Soc. Faraday Trans. 93 (3) (1997) 467–475.
[9] F. Manon Higgins, N.H. de Leeuw, S.C. Parker, J. Mater. Chem. 12 (2002) 124–131.
[10] A. Kirfel, G. Will, Acta Crystallogr B 36 (1980) 2881–2890.
[11] B.F. Pedersen, D. Semmingsen, Acta Crystallogr B 38 (1982) 1074–1077.
[12] P. Gallitelli, Period Mineral. 4 (1933) 1.
[13] N.N. Bushuev, V.M. Borisov, Russ. J. Inorg. Chem. 27 (1982) 341.
[14] W. Abriel, Acta Crystallogr. C 39 (1983) 956–958.
[15] G.A. Lager, Th. Armbruster, F.J. Rotella, J.D. Jorgensen, D.G. Hinks, Am. Mineral. 69 (1984) 910–918.
[16] A. Putnis, B. Winkler, L. Fernandez-Diaz, Min. Mag. 54 (1990) 123–128.
[17] P.P. Ewald, Ann. Phys. 64 (1921) 253.
[18] R.A. Jackson, Curr. Opin. Solid State Mater. Sci. 5 (2001) 463–467 doi: 10.1016/S1359-0286(01)00029-8.
[19] N.H. de Leeuw, S.C. Parker, Phys. Rev. B 58 (20) (1998) 901–908.
[20] B.G. Dick, A.W. Overhauser, Phys. Rev. B 112 (1958) 90.
[21] A. Pavese, M. Catti, G.D. Price, R.A. Jackson, Phys. Chem. Miner. 19 (1992) 80–87.
[22] J.D. Gale, J. Chem. Soc. Farad Trans. 93 (4) (1997) 629–637.
[23] S. Haussuhl, Z. Kristallogr. 122 (1965) 311–314.